E-Journal of Advanced Maintenance Vol.5 (2013) 175-184
Japan Society of Maintenology

Influence of Hydrogen in Steel on Oxidation Behavior of Low Carbon Austenitic Stainless Steel in High Temperature Water

Motoki NAKAJIMA[1,*], Shin-ichi KOMAZAKI [1,] and Tetsuo SHOJI[2]

[1] *Division of Mechanical Engineering, Graduate School of Science and Engineering, Kagoshima University, Kagoshima 890-0065, Japan*
[2] *Frontier Research Initiative, New Industry Creation Hatchery Center, Tohoku University, Sendai 980-8579, Japan*

ABSTRACT

The influence of hydrogen in steel on the high temperature water oxidation behavior of low carbon austenitic stainless steel Type F316L was investigated in order to clarify the mechanism of SCC initiation in the BWR environment, which is closely associated with the localized oxidation and its acceleration. The steel was charged with hydrogen by means of cathodic electrolysis. And then, the solution-treated (non-charged) and hydrogen-charged steels were subjected to the oxidation test in simulated BWR environment. Experimental results revealed that the size of outer oxide particle increased with increasing hydrogen content, resulting in the hydrogen accelerated oxidation (HAO). Additionally, the oxide of the hydrogen-charged steel was mainly $NiFe_2O_4$, whereas Fe_3O_4 was predominantly formed on the non-charged one. From the result of the small punch test in the BWR environment, it was also indicated that the effect of hydrogen on the oxidation might be almost equivalent to that of applied stress.

KEYWORDS

Oxidation, Low carbon austenitic stainless steel, High temperature water, Hydrogen, Stress corrosion cracking, Hydrogen accelerated oxidation

ARTICLE INFORMATION

Article history:
Received 31 July 2013
Accepted 12 November 2013

1. Introduction

The stress corrosion cracking (SCC) in a boiling water reactor (BWR) environment initiates after a long incubation period and then the crack grows abruptly. Therefore, it is strongly required to clarify the crack initiation mechanism from the viewpoint of aging management [1]. It has been reported that the localized metal oxidation and its acceleration play a primary role in crack initiation, especially, at the initial stage of SCC in the simulated BWR environment [2]. This localized oxidation affects the crack propagation as well as the initiation [1].

On the other hand, it has been known that the atmospheric and water vapor oxidations were accelerated by hydrogen in steel. The authors also have previously reported the influence of hydrogen content in steel on atmospheric oxidation behavior of low carbon austenitic stainless steel [3]. Experimental results revealed that relatively thick oxide films were formed on the hydrogen-charged specimen resulting in the hydrogen accelerated oxidation (HAO), when the hydrogen content was 35mass ppm. This HAO seemed to be closely associated with the decrease in Cr concentration in the inner oxide layer. Nakagawa et al. [4,5] investigated the corrosion behavior of heat-resistant ferritic steels in the steam/air multiphase environment, which simulated the environment of boiler tube in fossil power plant. The air side oxidation of high chromium ferritic steel (9-12%Cr steel) was more pronounced compared with the oxidation in ordinary air condition, although the oxidation rate on the air side was lower than that on the steam side. However, in the case of 2.25%Cr ferritic steel, the oxidation rate on the air side increased more significantly and resulted in being higher than that on the

[*]Corresponding author, E-mail: nakajima.motoki@jaea.go.jp
Present adress, *Blanket Technology Group, Blanket Research and Development Unit, Division of Fusion Energy Technology, Japan Atomic Energy Agency, Naka 311-0193, Japan*

Table 1 Chemical composition (mass%) and heat treatment condition of Type F316L.

C	Si	Mn	P	S	Ni	Cr	Mo	Fe
0.015	0.29	1.21	0.023	0.001	13.36	17.50	2.03	Bal.

1040-1052℃×157 min, water cooling

steam side to the contrary. These accelerated oxidation rates in the steam/air dual environment were lilely to be attributable to hydrogen, which was generated as a result of corrosion on the steam side and then permeated the steel toward the air side. Murata et al. [6] also observed the accelerated oxidation of high chromium ferritic steel, which was caused by hydrogen penetrated in oxide from water vapor.

However, in the case of high temperature and high pressurized water environments: *e.g.* BWR and PWR environments, information about the influence of hydrogen in metal on oxidation behavior was very limited. In the high temperature water, it have been considered that the hydrogen dissolved in water and hydrogen from metal corrosion can dissolve into the metal [7].

Hou et al. [7] performed the oxidation test on hydrogen-charged coupon-type specimen of Inconel Alloy 600 in high temperature water. They reported that the hydrogen in metal promoted the formation of oxide film in such environment also. But, the accelerated oxidation mechanism was not clearly clarified and the investigation concerning austenitic stainless steel Type F316L, which has been developed as the structural material for light water reactor, has not yet been reported.

In the present study, the low carbon austenitic stainless steel Type F316L was charged with hydrogen by means of cathodic electrolysis and then the hydrogen-charged steel was subjected to the oxidation test in simulated BWR environment to clarify the effect of hydrogen on oxidation. In addition, the small punch test was also carried out in the high temperature water to investigate the influence of applied stress on oxidation and examine a possible mechanism of accelerated oxidation.

2. Experimental Procedures

2.1. Materials and hydrogen charging condition

The material used in this study was low carbon austenitic stainless steel, Type F316L, which has been developed as the structural material for light water reactor. The chemical composition and heat treatment condition are shown in Table 1. The plate-type specimens with a dimension of 10×10×0.50 mm were used for the oxidation test. The specimen surface was finished by the colloidal silica.

The hydrogen charging into the specimens was conducted by means of cathodic electrolysis in H_2SO_4 aqueous solution (pH2.5, 80°C) containing 0.06 mass% NH_4SCN under a constant current density of 50 A/m^2. The charging times were 48 and 120 h. Next, in order to measure the hydrogen content in the steel, the thermal desorption spectroscopic (TDS) analyses were carried out at temperature range from room temperature to 500°C. The heating rate was 100°C/h.

2.2. Oxidation test

The oxidation tests were performed in the simulated BWR environment using an autoclave (Fig. 1), which was developed by the author's group for the small punch (SP) SCC test [8]. The autoclave was connected to the recirculation loop system in which the dissolved oxygen concentration and conductivity were adjusted. The temperature and the pressure were 288°C and 9 MPa, respectively. Dissolved oxygen (DO) concentration in the inlet water was kept being 2.0 ppm and its conductivity was <0.06 μS/cm. The tests were carried out under the water flow rate of inlet water at 0.5L/h. The specimens were exposed in the water for periods of 1~886 hours.

The SP tests with a constant load were also conducted using transmission electron microscope (TEM) disk-type specimen (ϕ3×0.25 mm) to investigate the effect of applied stress on oxidation behavior. The constant load of 200 N was applied to the center of the specimen, which was clamped between the upper and lower dies, through the Si_3N_4 ball (ϕ1.0 mm) using the electric servo motor

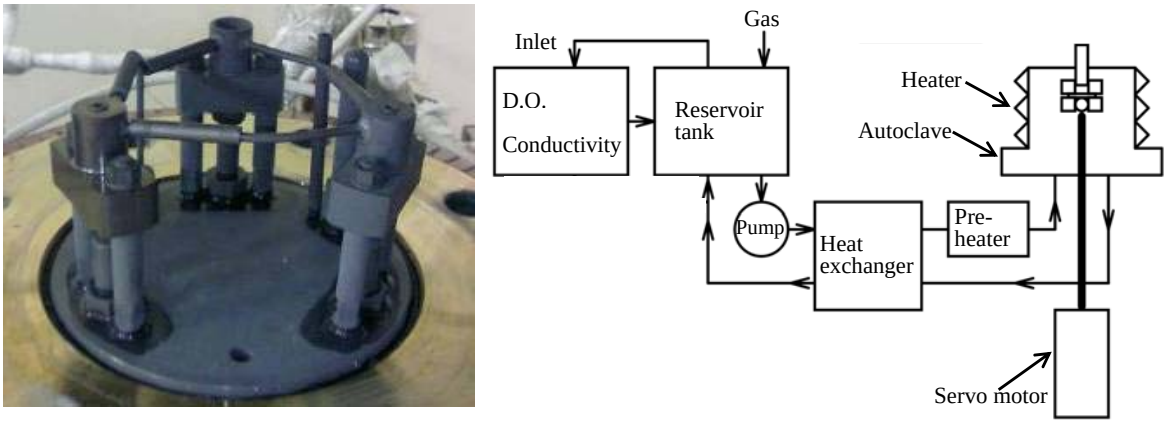

Fig. 1. Autoclave for SPSCC test and schematic illustration of the water recirculation loop system.

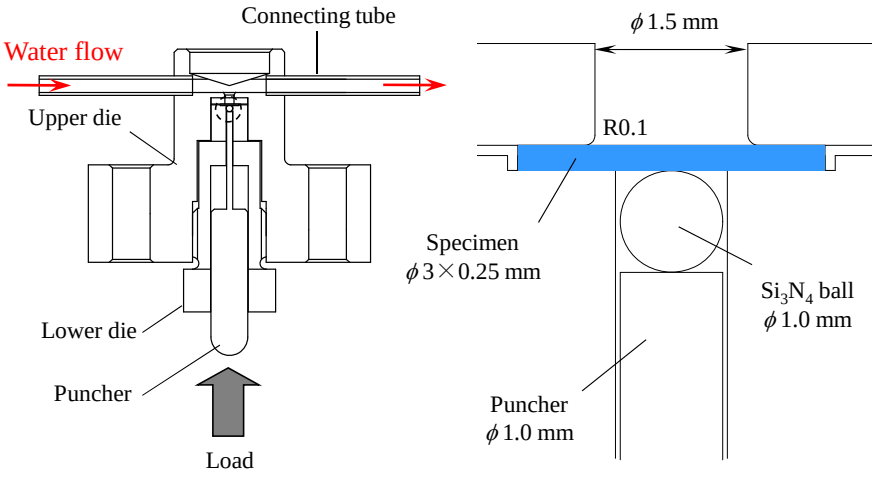

Fig. 2. Loading and specimen support configuration for the SPSCC test.

(Fig. 2) [9]. After the duration of 100 h, the oxidized surface of the SP test specimen (stress-applied specimen) were subjected to optical microscopy (OM), scanning electron microscopy (SEM), laser Raman spectroscopy (LRS) and X-ray photoelectron spectroscopy (XPS) analyses as well as the hydrogen-charged specimen.

3. Results and Discussion

3.1. Hydrogen desorption behavior of Type F316L

The hydrogen desorption curves measured on the solution-treated (non-charged) and the specimens charged for 48 and 120 h are given in Fig. 3, where the hydrogen evolution rate is plotted against temperature. There was no hydrogen evolution for the solution-treated. On the other hand, two clear large peaks appear at around 220 and 380°C in the profiles of hydrogen-charged specimens. The peak heights increase with increasing charging time. Hagi et al. [10] reported that the first and second peaks corresponded to the interstitial hydrogen in γ-phase and trapped hydrogen by dislocation, respectively. The hydrogen content was determined by calculating the area under each hydrogen profile. As the results, the specimens charged for 48 and 120 h contained hydrogen of 23 and 35 mass ppm, respectively.

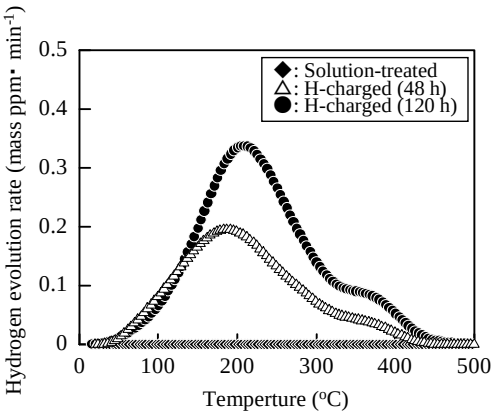

Fig. 3. Change in hydrogen evolution curves with hydrogen charging.

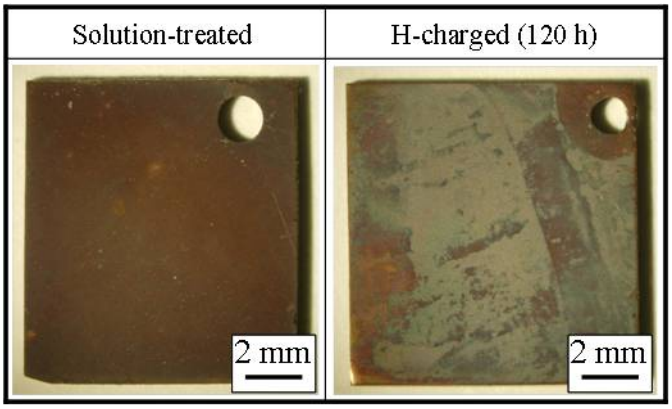

Fig. 4. OM images of oxidized samples.

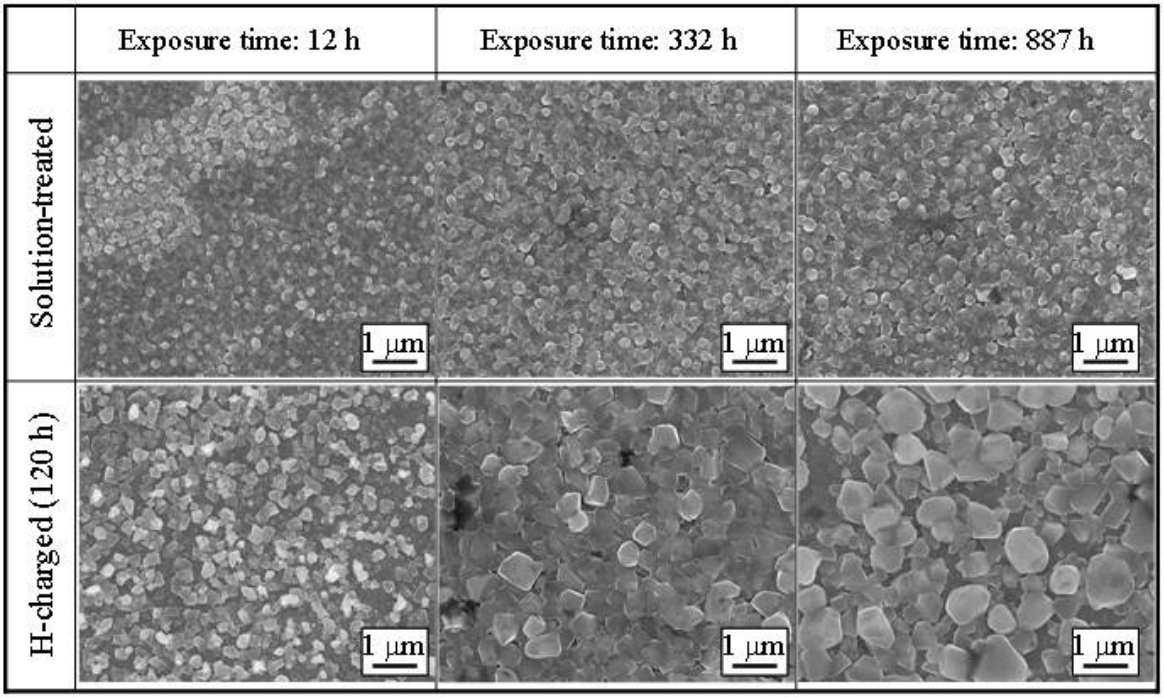

Fig. 5. Effects of hydrogen and exposure time on outer oxide layer.

3.2. Effect of hydrogen in steel on outer oxide scale character

Figure 4 shows the typical examples of the specimen surfaces of the solution-treated (non-charged) and the specimen charged for 120 h, which were taken after the oxidation tests (332 h) by optical microscope. It can be clearly seen that the color of specimen surface was significantly different between them. The oxidation was macroscopically homogeneous on the solution-treated specimen, whereas it was very inhomogeneous on the hydrogen-charged one. The SEM images of the specimen surfaces of the solution-treated and the hydrogen-charged (120 h) specimens, which were exposed in the simulated BWR environment for 12, 332 and 887 h, are given in Fig. 5. In both cases, the sizes of oxide particles increase as the exposure time increases. The growth of oxide particle was more pronounced in the initial stage of oxidation. As can be clearly seen in this figure, the oxide particle is remarkably enlarged by hydrogen in steel. That is to say, the oxidation of Type F316L in the simulated BWR environment is accelerated by hydrogen in steel (Hydrogen Accelerated Oxidation: HAO). Figure 6 shows the particle size measured on the solution-treated specimen and the specimens charged for 48 and 120 h plotted as a function of exposure time. The definition of particle size is also schematically illustrated in this figure. The particle sizes increase significantly at the initial stage of oxidation and after that they tend to increase gradually with exposure time, although some scattering results can be seen. It seems that their increases follow the parabolic or logarithmic law. There is an anomaly data point for the specimen charged for 120 h, when the exposure time 100 h. In addition, the scattering for the specimen is also larger than those for the other specimens. As can be seen in Fig. 4, the color on the specimen surface charged for 120 h is varied depending on the locations. The anomaly data and larger scattering seem to be caused by this macroscopic inhomogeneous oxidation behavior, because the averaged particle size was determined based on the results of only a few limited areas on such inhomogeneous surface.

Figure 7 shows the X-ray photoelectron spectroscopy (XPS) results of solution-treated and the hydrogen-charged (120 h) specimens oxidized for 332 h. The film thickness was defined as the sputtering depth of the half of the maximum oxygen concentration reaches. The film thickness of hydrogen-charged steel was around 700 nm, whereas that of solution-treated was only 250 nm. As can be seen in this figure, the Ni concentration of hydrogen-charged sample was higher than that of solution-treated one at the outermost layer.

In order to investigate the effect of hydrogen on the kind of oxide, the LRS analysis was performed. Figure 8 shows the results obtained from the solution-treated and the hydrogen-charged (120 h) specimens. In this figure, the peak position of oxide was cited the literature [11]. There is almost no difference irrespective of the exposure time in either case, however, the kind of oxide is different significantly between them. The oxide was mainly identified as $NiFe_2O_4$ at the hydrogen-charged specimen, whereas Fe_3O_4 was predominantly formed on the solution-treated one.

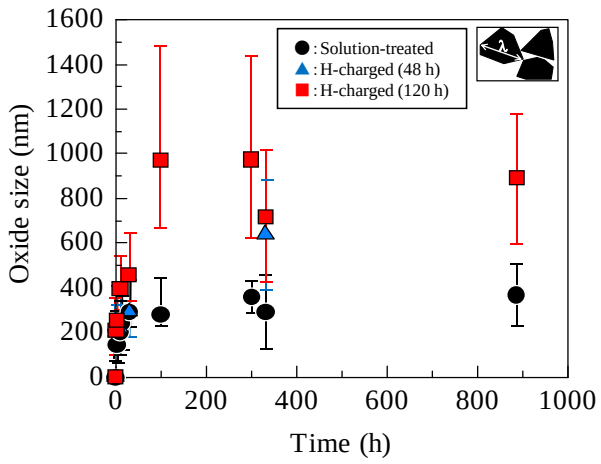

Fig. 6. Changes in oxide particle sizes with exposure time.

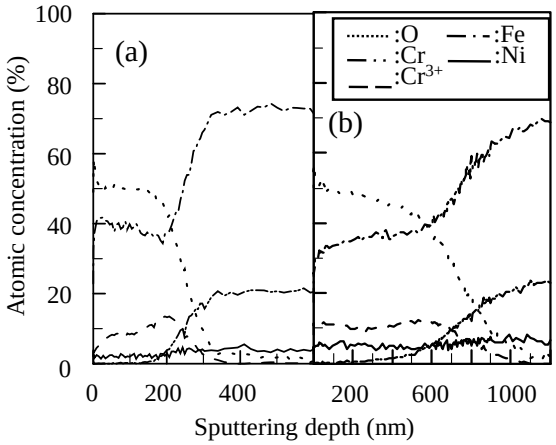

Fig. 7. XPS results of (a) non-charged and (b) hydrogen-charged samples.

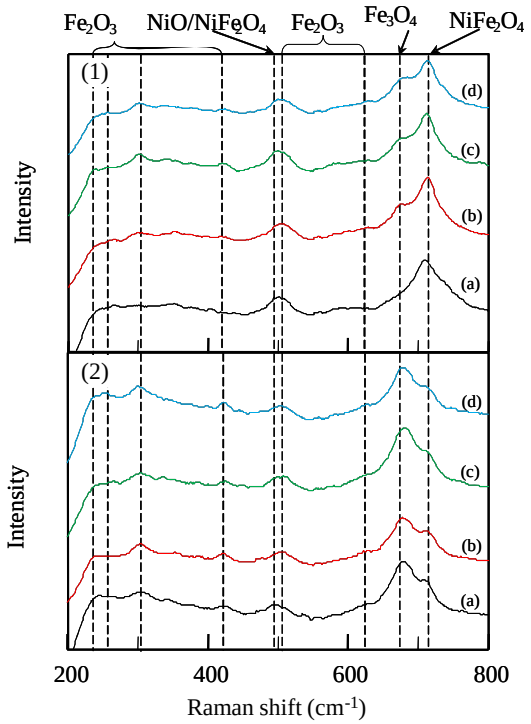

Fig. 8. Raman spectra of oxidized samples. (1) Hydrogen-charged (120 h). (2) Solution-treated. (a) 12 h. (b) 100 h. (c) 332 h. (d) 887 h.

3.3. Effect of applied stress on outer oxide particle character

The center (top) of the SP test specimen was also subjected to the above-mentioned analyses (Fig. 9). The finite element analysis (FEA) was necessary for investigating the effect of applied stress on oxidation behavior, because the stress and strain were not uniformly distributed on the specimen surface and were changed depending on the location of the specimen. Figure 10 shows the equivalent stress on the outer specimen surface plotted as a function of the distance from specimen center in addition to the deformation profile and the equivalent stress distribution. The equivalent stress reaches about 650 MPa around the center of the specimen, when the load is 200 N.

The SEM image of the outer oxide film formed on the center of the SP test specimen (the

stress-applied specimen) is given in Fig. 11 along with those of the solution-treated and the hydrogen-charged (120 h) specimens. The exposure times of those samples were fixed to be 100 h. As can be seen in this figure, the oxide particle formed on the stress-applied specimen is clearly larger than that on the solution-treated one and it is obvious from this result that the oxidation is accelerated by stress as well. However, the increase in particle size of the stress-applied specimen is less significant than that of the hydrogen-charged one. This result indicates that absorbed hydrogen is more effective in the acceleration of oxidation in the simulated BWR environment. Figure 12 shows the results of the LRS obtained from the stress-applied, the hydrogen-charged and the solution-treated specimens. $NiFe_2O_4$ is mainly formed on the stress-applied specimen as well as the hydrogen-charged one, although, as mentioned above, the principal oxide is Fe_3O_4 for the solution-treated specimen.

3.4. Discussion on possible mechanism of HAO

In this way, the hydrogen in steel and the applied stress have similar effects on the oxidation of Type F316L in the BWR simulated environment. In other words, the effect of hydrogen on oxidation may be almost equivalent to that of applied stress, because they both increase the particle size of outer oxide layer resulting in the accelerated oxidation and change the oxide type from Fe_3O_4 to $NiFe_2O_4$. It was considered that the acceleration of outer oxide growth was caused by the increase in metal ion transport in the inner oxide layer, because the outer oxide particle was formed by the deposition from the dissolved metal ions in the water.

Takeda et al. [12] measured the contact electric resistance (CER) of the oxide films formed on sensitized 304 stainless steel during the slow strain rate tensile test in the high temperature water. They observed the increase in CER value with strain and the accelerated oxidation. Based on the results, they concluded that vacancy formed in the oxide film under strain application was responsible for the increase in CER value and this vacancy facilitated the transport of metal ion in the oxide film resulting in the increase in oxidation rate. Some researchers [7, 13-16] reported that the dissolved hydrogen in the oxide increased concentration of ionic and electronic defects. Tveten et al. [15] has expected that the hydrogen in metals dissolves in the oxide film as interstitial protons. The protons in the oxide film are bonded to oxygen ions, forming substitutional hydroxide point defects. In addition, in order to remain electro-neutrally in the oxide, the vacancy was formed on the metal atomic position. Therefore, the dissolved interstitial protons in the film increase the concentration of metal vacancies in the film.Therefore, in the same way, hydrogen in steel seems to form vacancy in oxide film (inner oxide layer). The resultant vacancy is likely to play an important role as a preferential transport path of metal ions such as Ni and Fe ions. Needless to say, the increase in metal transport causes the larger particle size of outer oxide layer in the hydrogen-charged specimen. However, the cause of Ni enrichment at the outer layer has not yet been clarified. Further researches such as an investigation of the microstructure and chemical composition of the inner oxide layer and a measurement of its vacancy concentration would be necessary for discussing the HAO mechanism more quantitatively and/or in detail.

4. Summary

The oxidation test of the low carbon austenitic stainless steel Type F316L in simulated BWR environment was performed to clarify the effect of hydrogen on oxidation. In addition, the small punch test was also carried out in high temperature water for investigating the influence of stress on the outer oxide particle. From the present investigation, the following conclusions can be drawn.

1. The outer oxide particle size increases with hydrogen in steel. The oxidation of Type F316L in the simulated BWR environment is accelerated by hydrogen in steel (Hydrogen Accelerated Oxidation: HAO).
2. The oxide particle is mainly identified as $NiFe_2O_4$ on the hydrogen-charged steel, whereas Fe_3O_4 is predominantly formed on the non-charged one.
3. The oxidation is accelerated by stress as well. The effect of applied stress may be qualitatively consistent with that of hydrogen in steel.

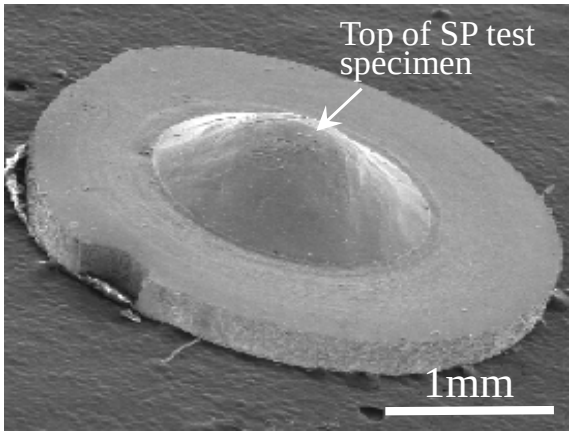

Fig. 9. SP test specimen.

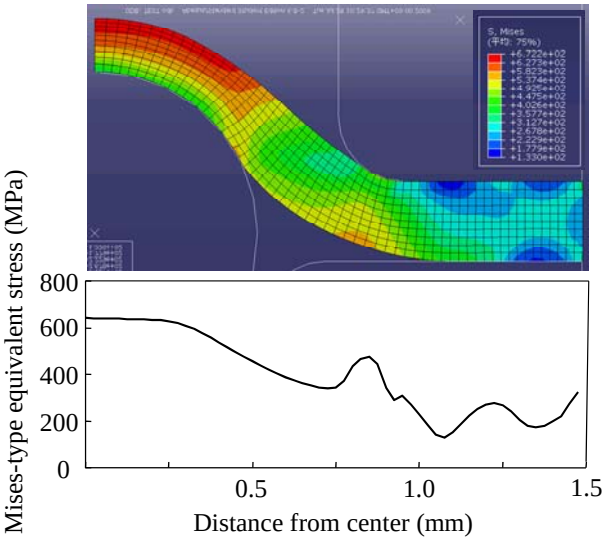

Fig. 10. FEA results of stress-applied sample.

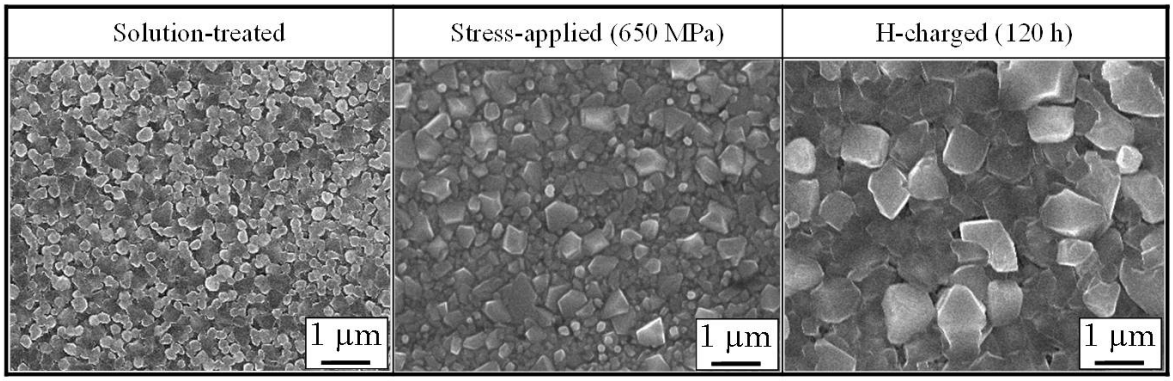

Fig. 11. SEM images of solution-treated, stress-applied and hydrogen-charged specimens after oxidation test for 100 h.

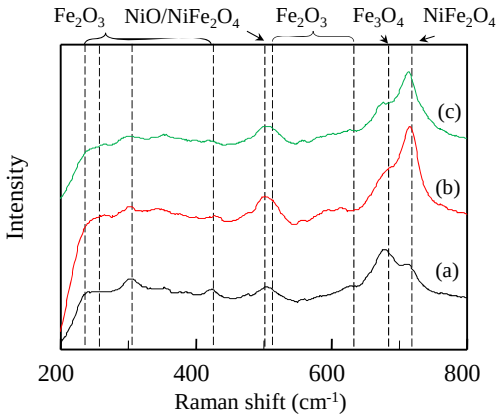

Fig. 12. Raman spectra of oxidized samples. (a) Solution-treated. (b) Stress-applied (c) Hydrogen-charged (120 h).

Acknowledgement

This work was performed as the part of the Project on Enhancement of Ageing Management and Maintenance of Nuclear Power Plants entrusted by Nuclear and Industrial Safety Agency (NISA) in the Ministry of Economy, Trade and Industry (METI) of Japan.

References

[1] Shoji, T., Research Activities of Stress Corrosion Cracking Session, ISaG2008, 24-25, July, 2008, The University of Tokyo, Tokyo, Japan.
[2] Wang, S., Shoji, T., and Kawaguchi, N., 2005, “Initiation of Environmentally Assisted Cracking in High-Temperature Water”, *Corrosion, Vol. 61*, pp. 137-144.
[3] Nakajima, M., Hosokawa, M., Komazaki, S., and Shoji, T., 2010, “Influence of Hydrogen Content in Steel on Atmospheric Oxidation Behavior of Low Carbon Austenitic Stainless Steel”, *Journal of the Japan Institute of Metals, Vol. 75*, pp. 243-247.
[4] Nakagawa, K., Matsunaga, Y., and Yanagisawa, T., 2001, “Corrosion Behavior of Ferritic Steels on the Air Sides of Boiler Tubes in a Steam/Air Dual Environment”, *Materials at High Temperatures, Vol. 18*, pp. 51-56.
[5] Nakagawa, K., Matsunaga, Y., and Yanagisawa, T., 2003, “Corrosion Behavior of Ferritic Steels on the Air Sides of Boiler Tubes in a Steam/Air Dual Environment”, *Materials at High Temperatures, Vol. 20*, pp. 67-73.
[6] Murata, Y., Nagai, K., Nakai, M., Kunieda, T., and Morinaga, M., 2007, “Relationship between High Temperature Steam Oxidation Resistance of Fe-Cr Alloys and the Dissolved Hydrogen Originated from the Steam”, *Journal of the Japan Institute of Metals, Vol. 71*, pp. 68-75.
[7] Hou, J., Peng, Q. J., Sakaguchi, K., Takeda, Y., Kuniya, J., and Shoji, T., 2010, “Effect of Hydrogen in Inconel Alloy 600 on Corrosion in High Temperature Oxygenated Water”, *Corrosion Science, Vol. 52*, pp. 1098-1101.
[8] Isselin, J., Wang, S., Komazaki, S., and Shoji, T., 2005, “Development of Small Punch Test for EAC Evaluation”, *Key Engineering Materials, Vol. 297-300*, pp. 980-985.
[9] Kato, T., Komazaki, S., Kohno, Y., Tanigawa, H., and Kohyama, A., 2009, “High-Temperature Strength Analysis of Welded Joint of RAFs by Small Punch Test”, *Journal of Nuclear Materials, Vols. 386-388*, pp. 520-524.
[10] Hagi, H., and Yanagawa, T., 2007, “Analysis of Hydrogen in Cathodically Polarized Austenitic Stainless Steels”, *Memoirs of the Fukui University of Technology, Vol. 37*, pp. 109-116.
[11] Furunushi, Y., and Masuda, M., 1999, "Thickness Evaluation of Thin Multilayered Scale by Glow Discharge Spectroscopy Associated with Raman Spectroscopy(Surface Analysis)", *Tetsu to Hagane, Vols.* 85, *pp.* 143-148.

[12] Takeda, Y., Masuda, T., and Shoji, T., "In-situ Measurement of Contact Electric Resistance of Oxide Films on Sensitized 304 Stainless Steel during Slow Strain Rate Test in High Temperature Water", Asian Pacific Conference on Fracture and Strength'01 and International Conference on Advanced Technology in Experiment Mechanics '01, 20-22, October, 2001, Sendai, Japan.
[13] Hultquist, G., Tveten, B., Hörnlund, E., Limbäck, M., Haugsrud, R., 2001, "Self-Repairing Metal Oxides", *Oxidation of Metals, Vol. 56*, pp. 313-346.
[14] Kofstad, P., 1995, "Defects and Transport Properties of Metal Oxides", *Oxidation of Metals, Vol. 44,* pp. 3-27.
[15] Tveten, B., Hultquist, G., and Norby, T., 1999, "Hydrogen in Chromium: Influence on the High-Temperature Oxidation Kinetics in O_2, Oxide-Growth Mechanisms, and Scale Adherence", *Oxidation of Metals, Vol. 52,* pp. 221-233.
[16] Norby, T., 1993, "Protonic defects in oxides and their possible role in high temperature oxidation", *Journal De Physique IV, Vol. 3,* pp. 99-105.